

Published in

Science and Technology for the Built Environment
Volume 23, 2017 - Issue 6: Purdue University Refrigeration Conference, Heat
and Mass Transfer

DOI:10.1080/23744731.2017.1325706

Title:

**Enhancement of R1234ze(Z) Pool Boiling Heat Transfer on Horizontal
Titanium Tubes for High-temperature Heat Pumps**

Author list:

Ryuichi NAGATA ¹
Chieko KONDOU ^{2,3*}
Shigeru KOYAMA ^{1,3}

¹ Interdisciplinary Graduate School of Engineering Sciences, Kyushu University,
6-1 Kasuga-koen, Kasuga, Fukuoka 816-8580, Japan

² Graduate School of Engineering, Nagasaki University
1-14 Bunkyo-machi Nagasaki 852-8521 Japan

³ NEXT-RP in International Institute for Carbon-Neutral Energy Research, Kyushu University,
744 Motoooka, Nishi-ku, Fukuoka 819-0395, Japan

* Corresponding author
Chieko Kondou, PhD
Associate Professor, Nagasaki University
Graduate School of Engineering, Division of System Science
1-14 Bunkyo-machi Nagasaki 852-8521 Japan
+81 95 819 2527 / ckondou@nagasaki-u.ac.jp

ABSTRACT

R1234ze(Z), which has a global warming potential of less than 1, is a promising alternative refrigerant for high-temperature heat pumps designed for heat recovery in the industrial sector. The use of titanium as the material for heat exchangers exposed to acid exhaust is one solution to prevent oxidation. In this study, the pool boiling heat transfer characteristics outside of horizontal titanium tubes were experimentally investigated for R1234ze(Z). A plain tube and three enhanced titanium tubes were tested at saturation temperatures from 10 to 60 °C and heat fluxes from 0.55 to 79.8 kW m⁻². Compared to the plain tube, the tested enhanced tube exhibited a 2.8 to 5.1 times higher heat transfer coefficient, on average, in the test range, which could compensate for the disadvantage in the thermal conductivity of titanium. The enhancement ratio predominantly depends on the saturation temperature and the wall heat flux. At conditions of higher saturation temperatures and lower heat flux, where smaller bubbles are observed, test tubes with smaller fin spaces exhibit higher heat transfer coefficients. The experimental results indicate the importance of fin geometry optimization to the operation conditions.

NOMENCLATURE

D_i	inner diameter	(m)
D_o	outer diameter	(m)
D_{root}	fin root diameter	(m)
L	active heat transfer length	(m)
M	molar mass	(g mol ⁻¹)
N	number of data	(-)
Q	heat transfer rate	(W)
R_a	arithmetic mean surface roughness	(μ m)
S	standard deviation	(%)
T	temperature	(°C)
\dot{V}	volumetric flow rate	(m ³ s ⁻¹)
c	specific heat	(J kg ⁻¹)
h	specific enthalpy	(J kg ⁻¹)
Δh_{LV}	latent heat of vaporization	(J kg ⁻¹)

p	pressure	(Pa)
p_{red}	reduced pressure	(-)
q	heat flux	(W m ⁻²)
α	heat transfer coefficient, HTC	(W m ⁻² K ⁻¹)
δ	tube thickness	(m)
$\bar{\varepsilon}$	relative bias	(%)
λ	thermal conductivity	(W m ⁻¹ K ⁻¹)
μ	viscosity	(Pa s)
ρ	density	(m ³ kg ⁻¹)
σ	surface tension	(Nm ⁻¹)

Subscript

0	reference value
Cu	copper
H ₂ O	water
L	saturated liquid
amb	ambient air
cal	calculated
exp	experimental
i	inside
in	inlet
loss	heat loss
m	average, middle
o	outside
out	outlet
sat	saturation state
tube	test tube
wall	tube wall
water	heating water

1. INTRODUCTION

Use of high GWP (global warming potential) refrigerants in air-conditioners and refrigeration systems became one of the international concerns for environment conservation. Shifting to the low GWP refrigerants is now urgent for the manufacturers. Cavallini et al. (2014) evaluated the performance potential of several conventional refrigerants, three natural refrigerants, and three hydro-fluoro-olefins: R1234yf, R1234ze(E), and R1234ze(Z). A set of 1200 low-GWP refrigerants with critical temperatures between 300 K and 400 K was assessed by McLinden et al. (2014), considering flammability, thermal stability, and toxicity for air conditioners. They concluded that no candidate refrigerant is ideal so far, however the surveillance range of the critical temperature can be increased for industrial high-temperature heat pumps. In the updated GWP list of IPCC 5AR, GWP_{100} of R1234ze(Z) is reported as less than one (e.g., Myhre et al., 2013; Hodnebrog et al., 2013). According to the assessment by Koyama et al. (2012), R1234ze(Z) is expected to be categorized as ASHRAE safety classification A2L (acute toxicity is less than the warning level and mildly flammable), and most metals, plastics, and elastomers are stable in this refrigerant. The equation of state was developed by Akasaka et al. (2014) on the basis of the measurement data by Higashi et al. (2015). Since then, R1234ze(Z) was nominated as a low-GWP alternative to R245fa ($GWP_{100} = 858$) because of its very similar thermodynamic properties and extremely low-GWP ($GWP_{100} < 1$), as listed in Table 1. The equation of state is available in REFPROP 9.1 (Lemmon *et al.*, 2013) and this accelerated the researches for R1234ze(Z). From the recently reported works (e.g., Fukuda et al., 2014; Longo et al., 2014), R1234ze(Z) is anticipated to be a promising candidate refrigerant for use in industrial high-temperature heat pumps. To reduce primary energy consumption, high-temperature heat pumps are applicable as heat recovery systems to assist steam boilers in the drying process of wood or paint, the distillation process of beverages, and the cleaning process of machined components (Kondou and Koyama, 2015).

In large-scale heat pumps, shell-and-tube heat exchangers made of copper are most widely used. However, the heat exchangers of such heat pumps designed for waste heat recovery systems are often exposed to exhaust containing acidic substances. Using titanium as the material is one solution to prevent oxidation in the polluted exhaust. Titanium is also advantageous to reduce the weight of large heat exchangers for shipping and installation and to reduce costs if the wall thickness is sufficiently reduced relative to copper tubes. As comprehensively reviewed (e.g., Pate et al., 1990, Webb, 1994; Thome, 2006), numerous enhancement techniques have been patented and some have been applied to the pool boiling of the shell-and-tube heat exchangers. The most common technique is a surface with dense re-entrant cavities produced by a mechanically deformed copper low-finned tube. Similar attempts were made with the titanium tubes in this study.

The pool boiling heat transfer characteristics outside of enhanced, horizontally oriented, titanium tubes are experimentally investigated for R1234ze(Z). A plain tube and three enhanced tubes with different re-entrant cavities are tested in a pressure vessel, and the boiling behavior is observed to determine the optimum tube geometry for R1234ze(Z) at relatively higher saturation temperatures for waste heat recovery.

2. EXPERIMENTS

2.1 Experimental setup

Fig. 1 shows the experimental apparatus used to characterize the R1234ze(Z) pool boiling outside the titanium tubes. This apparatus consists of cooling and heating water loops connected to temperature control baths and a refrigerant loop of natural circulation driven by gravity. The main components of the refrigerant loop are a condenser and an evaporator. In the evaporator, the horizontally oriented test tube is immersed in liquid R1234ze(Z) that flows down from the condenser; meanwhile, heating water flows through the test tube. The test tubes are observed through a glass window set in the evaporator during the experiment. The temperature of liquid R1234ze(Z) is measured by thermocouples near the test tube to confirm the state can be justified as saturation. The inlet and outlet temperatures of the heating water are measured in the mixing chambers by Pt thermometers with uncertainty of ± 0.05 K. The volumetric flow rate is measured with a gear type meter installed in the water loop with uncertainty of $\pm 0.5\%$ of the reading value. The instrument and the measurement uncertainties are summarized in Table 2. The temperature change in the heating water over the test tube is kept at 3 K to suppress the tube wall temperature distribution within 2 K. The tube wall temperature is measured by an electric resistance method. As illustrated in Fig. 1 (b), the test tube is electrically insulated by an applied constant direct current. The voltage drop of test tube over the heat transfer length is measured and correlated to the tube wall temperature. During the calibration, the evaporator chamber is vacuumed and the heating water is supplied at a maximum flow rate for reducing the temperature distribution. Fig. 2 (a) shows the example of the calibration data. The horizontal axis shows the tube wall temperature, which is assumed equal to the average water temperature, and the horizontal axis shows the electric resistance of tube wall over the heat transfer length. From the calibration, it was confirmed that the correlation of the voltage drop is almost proportional to the temperature and is able to predict the temperature

within ± 0.1 to 0.24 K for each test tube. The saturation pressure of R1234ze(Z) is adjusted by controlling the temperature and flow rate of the cooling water delivered to the condenser and is measured by an absolute pressure transducer within ± 0.14 kPa. The heat flux condition is adjusted by controlling the flow rate of the heating water. The active heat transfer length of the test tube is 400 mm; the resistance (voltage drop) measurement length is 396 mm. Table 3 lists the dimensions of the test tubes; two plain tubes made of copper and titanium and three enhanced titanium tubes TE01, TE02, and TE03 were used. The depth and inner width of the reentrant cavities, which are measured with cut surfaces of the sample tube, range approximately from 0.375 mm to 0.410 mm and from 0.270 mm to 0.310 mm, respectively. Although the considerable variation is found from the measurement at random positions, those are common for the three test tubes. The most distinct difference of these enhanced tubes is the open mouth width. The axial open mouth widths are 0.084 ± 0.015 mm for TE01, 0.143 ± 0.016 mm for TE02, and 0.171 ± 0.020 mm for TE03. The open mouth width of tube TE01 is the narrowest and that of TE03 is the widest.

2.2 Data reduction

The heat transfer rate over the test tube is obtained from the heat balance of the heating water as,

$$Q_{\text{H}_2\text{O}} = \dot{V}_{\text{H}_2\text{O}} \rho_{\text{H}_2\text{O}} (h_{\text{H}_2\text{O},\text{in}} - h_{\text{H}_2\text{O},\text{out}}) - Q_{\text{loss}} \quad (1)$$

where $h_{\text{H}_2\text{O},\text{in}}$ and $h_{\text{H}_2\text{O},\text{out}}$ are the enthalpy of the heating water obtained from the measured bulk mean temperature at the inlet and outlet of the test tube. Q_{loss} is the heat leaked to the ambient, which is correlated to the temperature difference between the heating water and ambient air, as shown in Fig. 2 (b). At a typical condition of the temperature difference 10 K, the heat leak is approximately 7 W, which corresponds approximately 3% of total heat transfer rate at a heat flux of 10 kWm⁻². The average heat flux q_{wall} is defined with the outer surface for the plain test tube and with the apparent outer surface at the fin tip diameter for the enhanced tubes.

$$q_{\text{wall}} = Q_{\text{H}_2\text{O}} / (\pi D_o L) \quad (2)$$

where L is the active heat transfer length of 400 mm. The above is average heat flux for the tube length, varying from one end to the other with the water temperature variation of within 3 K.

The tube wall temperature $T_{\text{wall,m}}$ measured by the resistance method is assumed to correspond to the average wall temperature over the internal surface to the fin root. Considering the heat conduction through the tube wall, the reference tube wall temperature at the fin root T_{wall} is corrected by the following equation.

$$T_{\text{wall}} = T_{\text{wall,m}} - \frac{Q_{\text{H}_2\text{O}} \ln(D_{\text{root}}/D_{\text{m}})}{2\pi\lambda_{\text{tube}}L}, \quad D_{\text{m}} = \frac{(D_{\text{root}} + D_{\text{i}})}{2} \quad (3)$$

For the plain tube, the fin root diameter D_{root} is substituted by the outer diameter D_{o} . λ_{tube} is the thermal conductivity of the tube wall. For the copper tube, the value $385 \text{ W m}^{-1}\text{K}^{-1}$ is applied. For titanium tubes, the value provided from the manufacturer of $18.9 \text{ W m}^{-1}\text{K}^{-1}$ is applied in this study. The water temperature change from inlet to outlet is kept within 3 K. Thus, the temperature distribution of the test tube wall in the flow direction can be suppressed within 2 K over the entire test range. The relative value of the tube wall temperature distribution to the superheat was maximized at the smallest wall superheat; nevertheless, the value was within 13%.

Finally, the average heat transfer coefficient (HTC) is given as,

$$\alpha = q_{\text{wall}} / (T_{\text{wall}} - T_{\text{sat}}) \quad (4)$$

where T_{sat} is the saturation temperature of R1234ze(E). The thermodynamic and transport properties of R1234ze(Z) and water are calculated by REFPROP 9.1.

3. RESULTS AND DISCUSSION

3.1 Plain tubes – copper and titanium tubes

First, the differences between copper and titanium tubes are compared with the experimental results of plain tubes. As listed in Table 3, the distinct differences of these two tubes are the surface roughness, wall thickness, and thermal conductivity. Because the extensibility of the titanium alloy is not as high as that of copper alloy, the surface of titanium tubes tends to be much rougher than that of copper tubes. On rougher surfaces, the presence of larger embryonic bubble diameters produced by increased vapor entrapment in the micro cavities primarily enhances nucleated boiling (Rainey and You, 2000). However, the thicker tube wall and lower thermal conductivity of titanium tubes increases the thermal resistance over the tube wall. The thermal resistance of the copper tube and titanium tubes, $1/(\delta\lambda_{\text{tube}})$, are approximately 2.36 KW^{-1} and 26.45 KW^{-1} , respectively. The thermal resistance of the titanium tube is 11 times that of the copper tube, which completely compensates for the advantage

of surface roughness. For copper tubes, the temperature difference from the internal to outer surface is approximately 0.05 K. Thus, the tube wall thermal resistance is negligible. For the test titanium tube, at a heat flux of 20 kWm⁻² and a saturation temperature of 30 °C, the temperature difference between the internal and outer surfaces is 1.9 K. At this condition, the average wall superheat, $T_{\text{wall}} - T_{\text{sat}}$, is 3.9 K. Therefore, the tube wall thermal resistance takes 33% of the resistance from the internal surface to the boiling site. Therefore, for titanium tubes, reducing the tube wall thickness with consideration of corrosion is important.

Fig. 3 shows the experimentally quantified pool boiling HTC on plain tubes of copper and titanium at saturation temperatures T_{sat} of 10, 30, and 60 °C as a function of the heat flux. The horizontal and vertical bars appended to the symbols indicate the measurement uncertainty of 95 % coverage (Taylor, 1997). As plotted in Fig. 3, at a saturation temperature of 10 °C, HTC on the titanium tube is higher than that of the copper tube. At a saturation temperature of 60 °C, the HTC of the copper tube exceeds that of the titanium tube. The increased ratio of the HTC to heat flux of the copper tube is greater than that of the titanium tube. Therefore, the HTC of the copper tube is more sensitive to the saturation temperature and heat flux than that of the titanium tube.

In Fig. 3, the correlations of Gorenflo et al. (2010) and Ribatski-Jabardo (2003) are also plotted.

Gorenflo et al. (2010):
$$\alpha = \alpha_0 F_{q_{\text{wall}}} F_{p_{\text{red}}} F_R F_{w_m} \quad (5)$$

where $\alpha_0 = 3.58 \left[\left(\frac{dp}{dT} \right)_{\text{sat}} / \sigma \right]^{0.6}$ at $p_{\text{red}} = 0.1$. $F_{q_{\text{wall}}} = (q_{\text{wall}} / q_{\text{wall}0})^{(0.95 - 0.3 p_{\text{red}}^{0.3})}$, $q_{\text{wall}0} = 20$ [kWm⁻²].

$$F_{p_{\text{red}}} = 0.7 p_{\text{red}}^{0.2} + 4 p_{\text{red}} + (1.4 p_{\text{red}}) / (1 - p_{\text{red}}). \quad F_R = (R_a / R_{a0})^{2/15}, \quad R_{a0} = 0.4 \text{ } [\mu\text{m}].$$

$$F_{w_m} = \left[(\rho_{\text{tube}} c_{\text{tube}} \lambda_{\text{tube}}) / (\rho_{\text{Cu}} c_{\text{Cu}} \lambda_{\text{Cu}}) \right]^{0.25}.$$

Ribatski-Jabardo (2003):
$$\alpha = f_{w_m} (q_{\text{wall}}^{0.9 - 0.3 p_{\text{red}}^{0.2}}) p_{\text{red}}^{0.45} [-\log(p_{\text{red}})]^{-0.8} R_a^{0.2} M^{-0.5} \quad (6)$$

where M is the molar mass of the refrigerant. The material parameters are recommended as $f_{w_m}=100$ for copper, $f_{w_m}=110$ for brass, and $f_{w_m}=85$ for stainless steel. For the titanium tube, f_{w_m} is assumed as 90 because the thermophysical properties of titanium alloy are similar to stainless steel. For instance, the temperature diffusivities of copper alloy, titanium alloy, and stainless steel are, respectively, 95, 6.7, and 4.1 m² s⁻¹. Additionally, the bias is minimized at a material parameter f_{w_m} of 90.6.

Table 4 compares the selected correlations to the experimental results for the copper tube and the titanium tubes.

The relative bias, $\bar{\varepsilon}$, and the standard deviation S are introduced to quantify the degree of agreement.

$$\bar{\varepsilon} = \frac{1}{N} \sum_{j=1}^N \varepsilon_j = \frac{1}{N} \sum_{j=1}^N \left(\frac{\alpha_{\text{exp}} - \alpha_{\text{cal}}}{\alpha_{\text{cal}}} \times 100 \right) \quad [\%] \quad (7)$$

$$S = \sqrt{\frac{1}{N} \sum_{i=1}^N (\varepsilon_i - \bar{\varepsilon})^2} \quad [\%] \quad (8)$$

where N is the number of data. Among the selected correlations, the correlations of Gorenflo et al. (2010) and Ribatski-Jabardo (2003) show the best agreement with the experimental HTC for the copper tube and the titanium tube, respectively. Nevertheless, the Grenflo et al. (2010) correlation deviates from the experimental HTC of the titanium tube because the f_{wm} in Eq. (5) is not validated for titanium. The same material inherent properties affect nucleate boiling. For instance, temperature diffusivity determines the recovery speed of the wall superheat of the spot where the nucleate bubble departed. The surface energy determines the wettability and wickability and affects the shape of nucleate bubbles. For instance, Phan et al. (2009) demonstrated that the highest HTC was appeared with a surface having the highest wettability for pool boiling on horizontally oriented plain heat transfer surfaces. The temperature recovery speed and surface wettability would considerably affect the pool boiling on horizontal tubes. However, to discuss the effects of the material dependence on nucleate HTC, a further approach and comprehensive database are needed.

3.2 Enhanced titanium tubes

Fig. 4 shows the variation of R1234ze(Z) pool boiling HTC on the enhanced titanium tubes: TE01, TE02, and TE03 at saturation temperatures of 10, 30, and 60 °C. TE01 has the narrowest opening of the small tunnels underneath the fin-tip surface; TE03 has the widest opening moth. The symbols indicate the experimental HTC of the enhanced tubes, whereas the dashed line indicates the predicted HTC by Ribatski-Jabardo (2003) of the titanium plain tube.

The enhanced tube TE01 with narrowest opening exhibits much higher HTC than the plain tube, even at lower heat flux. At the saturation temperatures of 10 and 30 °C, TE01 shows a slight decrease in HTC with increasing heat flux. At a saturation temperature of 60 °C, the HTC of TE01 increases at heat fluxes up to 10 kWm⁻² and then plateaus. This HTC behavior of TE01 is different than the plain tube. In contrast, the enhanced tube TE03 shows similar tendency to the plain tube. The HTC of TE03 monotonically increases with increasing heat flux.

At heat fluxes above 50 kWm⁻², the HTC increment ratio to heat flux seems to decrease slightly. Thus, under the conditions of higher heat fluxes, the HTC of TE03 exceeds that of TE01.

The predicting correlation is proposed by VanRooyen and Thome (2013) for pool boiling of R134a, R236fa, and R1234ze(E) on enhanced copper tubes.

$$\alpha = 967 \left(l_H / \delta_a \right)^{1.06} \left(\lambda_L / D_o \right) \left(l_H / \delta_a \right) = \left(\frac{8.6 \times 10^{-21}}{T_{\text{wall}} - T_{\text{sat}}} \right)^{1/3} \frac{(\rho_L \Delta h_{LV})^{2/3}}{(\lambda_L \mu_L)^{1/2} (T_{\text{sat}} + 273.15)^{1/6}} \quad (9)$$

The coefficient 967 and the exponent 1.06 are empirical parameters obtained for one of their test tube. The HTC calculated by the above correlation with the thermophysical properties of R1234ze(Z) is referred in Fig. 4. The calculated HTC, plotted with thin solid line in Fig. 4, is significantly higher than the experimentally obtained HTC and does not show the obvious variation against saturation temperature. The boiling HTC of R1234ze(Z) on the tested titanium tubes is more greatly affected by change in thermophysical properties.

Fig. 5 shows the boiling behavior of R1234ze(E) at a temperature of 30 °C on the tested titanium tubes. The upper row shows the vapor bubbles at a heat flux of 7 kWm⁻²; while the lower row shows the same at a heat flux of 70 kWm⁻². At a lower heat flux of 7 kWm⁻², the reentrant cavities of TE01 discharges greater number and larger size of bubbles, relative to TE02 and TE03. This bubble behavior supports the HTC data shown in Fig. 4 (b) that points TE01 exhibits much higher HTC at lower heat fluxes. On the other hand, at a heat flux of 70 kWm⁻², the bubbles on TE01 are larger than that on the other tubes and appears to coalesce each other. The bubbles on TE03 seems finer and numerous relative to the other two enhanced tubes. This suggests the frequency of bubble discharge from the cavities is higher than the others, and can explain the reason that TE03 exhibits the highest HTC at heat fluxes above 50 kWm⁻².

Fig. 6 compares the HTC enhancement ratio based on the plain titanium tubes, $\alpha_{\text{enhanced}} / \alpha_{\text{plain}}$, between TE01, TE02, and TE03. The parenthesized numbers in the symbol legend indicate the average value. The enhancement ratio ranges widely from 13 to 2. Over the entire range of the experiment, the tested tubes yield an enhancement ratio more than double. The enhancement ratio is significant at lower heat flux; then, the ratio decreases as the heat flux increases. The tunnel structures are beneficial at the early stage of nucleate boiling. The decrement is greater for TE01 but moderate for TE03 changing, the enhancement ratios of TE01 and TE03. In general, at lower

saturation temperatures, most fluids show lower nucleate boiling HTC due to their greater surface tension. Under such conditions, the tunnel structures of the narrow opening are more beneficial to enhance boiling heat transfer.

The narrow opening is advantageous at lower heat flux and lower saturation temperatures. From the observation of the bubble behavior, the following results are found. Because the narrow opening eases the holding of liquid refrigerant in the tunnels and increases the degree of superheat in the micro cavities inside the tunnels, this geometry yields acceleration of the boiling incipience and the nucleate boiling. However, at higher heat fluxes, the bubbles are generated faster and they stretch out in the tunnels until they depart from the tunnel mouth. The narrow opening interferes with the emerging vapor in the tunnels and the ingress of liquid to the tunnels. Some portion of the internal surface of the tunnels is dried-out. Thus, the enhancement ratio of the boiling heat transfer drastically decreases. These findings coincide with some remarks in previous studies by Nakayama et al. (1980a, 1980b) and also by Chien and Webb (1998)

4. CONCLUSIONS

Pool boiling heat transfer characteristics outside of horizontal titanium tubes were investigated for industrial high-temperature heat pumps designed for waste heat recovery. The R1234ze(Z) pool boiling heat transfer coefficients on a plain tubes and three enhanced tubes were experimentally quantified. The main findings are the following:

- On titanium tubes, thermal resistance over the tube wall is large due to lower thermal conductivity. Thus, reducing the tube wall thickness with consideration of corrosion is important when using titanium tubes.
- Among the selected correlations, Gorenflo et al. (2010) showed the best agreement with the experimental data of the plain copper tube. Nevertheless, this correlation considerably deviated from the data of titanium plain tubes because the material parameter used in this correlation is not valid for titanium tubes. The Ribatski-Jabardo (2003) correlation with a material parameter of 90 has the best agreement with the plain titanium tube.
- Enhanced titanium tubes with tunnels produced by mechanically deforming low-finned tubes exhibited HTC enhancement ratios based on the titanium plain tube from 13 to 2 over the entire experimental range. The opening width significantly changed the enhancement ratio. To optimize this parameter for a refrigerant, the saturation temperature and heat flux are important.

- At lower saturation temperatures and lower heat fluxes, the enhanced tube with the narrowest opening had the highest HTC. The narrower opening eases the holding of liquid and increases the degree of superheating in the tunnels, which accelerates the boiling incipience and nucleates boiling.
- At higher saturation temperatures and higher heat fluxes, the enhanced tube with the widest opening had the highest HTC. The wide opening helps emerging bubbles to depart from the tunnels and the ingress of liquid into the tunnels.

ACKNOWLEDGEMENTS

The present study is sponsored by the project on the "Development of High Efficiency and Non-Freon Air Conditioning Systems" of the New Energy and Industrial Technology Development Organization (NEDO) Japan. The tested refrigerant R1234ze(Z) was kindly supplied by Central Glass Co., Ltd. The tested tubes were kindly provided by Shinko Metal Products Co., Ltd.

REFERENCES

- ASHRAE, 2015. SSPC-34 : Designation and Safety Classification of Refrigerants. ANSI/ASHRAE Standard 34-2013 Addenda 2015.
- Akasaka, R., Higashi, Y., Miyara, A., Koyama, S., 2014. A fundamental equation of state for cis-1,3,3,3-tetrafluoropropene (R-1234ze(Z)). *Int. J. Refrig.* 44, 168–176. doi:10.1016/j.ijrefrig.2013.12.018
- Brown, J.S., Zilio, C., Cavallini, A. (2009). The fluorinated olefin R-1234ze(Z) as a high-temperature heat pumping refrigerant. *Int. J. Refrig.*, 32, 1412–1422. doi:10.1016/j.ijrefrig.2009.03.002
- Cavallini, A., Zilio, C., Brown, J.S., 2014. Sustainability with prospective refrigerants. *Energy Res.* 38, 285-298.
- Chien, L.H., Webb, R.L. (1998a). Visualization of pool boiling on enhanced surface. *Exp. Therm. Fluid Sci.*, 16, 332-341.
- Chien, L.H., Webb, R.L. (1998b). A parametric study of nucleate boiling on structured surfaces, Part1: Effect of tunnel dimensions", *Trans. ASME, J. Heat Transf.*, 120, 1042-1048.
- Chien, L.H., Webb, R.L. (1998c). A parametric study of nucleate boiling on structured surfaces, Part2: Effect of pore diameter and pore pitch", *Trans. ASME, J. Heat Transf.*, 120, 1049-1054.
- Fukuda, S., Kondou, C., Takata, N., Koyama, S., 2014. Low GWP refrigerants R1234ze(E) and R1234ze(Z) for high temperature heat pumps. *Int. J. Refrig.* 40, 161–173. doi:10.1016/j.ijrefrig.2013.10.014
- Gorenflo, D., Baumhögger, E., Windmann, T., Herres, G., (2010). Nucleate pool boiling, film boiling and single-phase free convection at pressures up to the critical state. Part I: Integral heat transfer for horizontal copper cylinders. *Int. J. Refrig.*, 33, 1229–1250. doi:10.1016/j.ijrefrig.2010.07.015
- Higashi, Y., Hayasaka, S., Shirai, C., Akasaka, R., 2015. Measurements of P_vT properties, vapor pressures, saturated densities, and critical parameters for R 1234ze(Z) and R 245fa. *Int. J. Refrig.* 52, 100–108. doi:10.1016/j.ijrefrig.2014.12.007
- Hodnebrog, Ø., Etminan, M., Fuglestedt, J.S., Marston, G., Myhre, G., Nielsen, C.J., Shine, K.P., Wallington, T.J., 2013. Global warming potentials and radiative efficiencies of halocarbons and related compounds: A comprehensive review. *Rev. Geophys.* 51, 300–378. doi:10.1002/rog.20013

- Jung, D., Kim, Y., Ko, Y., Song, K., (2003). Nucleate boiling heat transfer coefficients of pure halogenated refrigerants. *Int. J. Refrig.*, 26, 240–248.
- Kondou, C., Koyama, S. (2015). Thermodynamic assessment of high-temperature heat pumps using Low-GWP HFO refrigerants for heat recovery. *Int. J. Refrig.*, 53, 126–141. doi:10.1016/j.ijrefrig.2014.09.018
- Kondou, C., Nagata, R., Nii, N., Koyama, S., Higashi, Y., 2015. Surface tension of low GWP refrigerants R1243zf, R1234ze(Z), and R1233zd(E). *Int. J. Refrig.* 53, 80–89. doi:10.1016/j.ijrefrig.2015.01.005
- Koyama, S., Higashi, T., Miyara, A., Akasaka, R., 2013. Research and development of low-GWP refrigerants suitable for heat pump systems. In: JSRAE Risk Assessment of Mildly Flammable Refrigerants-2012 Progress Report, pp. 29-34
- Lemmon, E.W., Huber, M.L., McLinden, M.O. (2013). Reference Fluid Thermodynamic and Transport Properties - REFPROP Ver. 9.1. National Institute of Standards and Technology, Boulder, CO, USA.
- Longo, G.A., Zilio, C., Righetti, G., Brown, J.S., Experimental assessment of the low GWP refrigerant HFO-1234ze(Z) for high temperature heat pumps, *Experimental Thermal And Fluid Science*, 2014, vol. 57, 293–300.
- Myhre, G., Shindell, D., Bréon, F.-M., Collins, W., Fuglestedt, J., Huang, J., Koch, D., Lamarque, J.-F., Lee, D., Mendoza, B., Nakajima, T., Robock, A., Stephens, G., Takemura, T., Zhan, H., 2013. 2013: Anthropogenic and Natural Radiative Forcing, in: *Climate Change 2013: The Physical Science Basis. Contribution of Working Group I to the Fifth Assessment Report of the Intergovernmental Panel on Climate Change.* doi:10.1017/CBO9781107415324.018
- Nakayama, W., Daikoku, T., Kuwahara, H., Nakajima, T. (1980a). Dynamic model of enhanced boiling heat transfer on porous surfaces. Part1: Experimental investigation, *Trans. ASME, J. Heat Transf.*, 102, 445-450.
- Nakayama, W., Daikoku, T., Kuwahara, H., Nakajima, T. (1980b). Dynamic model of enhanced boiling heat transfer on porous surfaces. Part2: Analytical modeling, *Trans. ASME, J. Heat Transf.*, 102, 451-456.
- Pate, M.B., Ayub, Z.H., Kohleer, J., (1990). Heat Exchangers in the Air Condition and Refrigeration Industry, *Compact Heat Exchangers*, Shah, R.K., Kraus, A.D., Metzger, D.E., eds., Hemisphere, New York, 567-590.
- Phan, H.T., Caney, N., Marty, P., Colasson, S., Gavillet, J., 2009. Surface wettability control by nanocoating: The effects on pool boiling heat transfer and nucleation mechanism. *Int. J. Heat Mass Transf.* 52, 5459–5471.
- Rainey, K.N., You, S.M. (2000). Pool Boiling Heat Transfer From Plain and Microporous, Square Pin-Finned Surfaces in Saturated FC-72. *Int. J. Heat Transf.*, 122, 509-516.
- Ribatski, G., Jabardo, J.M.S., 2003. Experimental study of nucleate boiling of halocarbon refrigerants on cylindrical surfaces. *Int. J. Heat Mass Transf.* 46, 4439–4451.
- Stephan, K., Abdelsalam, M. (1980). Heat-Transfer Correlations for Natural Convection Boiling. *Int. J. Heat Mass Transf.*, 23, 73–87.
- Taylor, J.R. (1997). An introduction to error analysis, second ed. University science book, 73-77.
- Thome, J.R. (2006). Ch. 9: Boiling Heat Transfer on External Surfaces. *Engineering Data Book III*, Wolverine Tube, Inc., 1-38.
- Van Rooyen, E., Thome, J.R., 2013. Pool boiling data and prediction method for enhanced boiling tubes with R-134a, R-236fa and R-1234ze(E). *Int. J. Refrig.* 36, 447–455. doi:10.1016/j.ijrefrig.2012.11.023
- Webb, R.L. (1994). Ch. 11, *Principles of Enhanced Heat Transfer*, N Y, Wiley.

Captions:

Figure 1: Experimental apparatus.

- (a) Water and refrigerant loop
- (b) The evaporator chamber without insulation
- (c) Structure of the test section

Figure 2: Determination of wall temperature and heat loss

- (a) calibration curve for wall temperature
- (b) correlation for the heat loss

Figure 3: Variation of R1234ze(Z) pool boiling HTC on the test tubes of plain copper and titanium.

- (a) $T_{\text{sat}} = 10 \text{ }^{\circ}\text{C}$
- (b) $T_{\text{sat}} = 30 \text{ }^{\circ}\text{C}$
- (c) $T_{\text{sat}} = 60 \text{ }^{\circ}\text{C}$

Figure 4: Variation of R1234ze(Z) pool boiling HTC on the enhanced titanium tubes.

- (a) $T_{\text{sat}} = 10 \text{ }^{\circ}\text{C}$
- (b) $T_{\text{sat}} = 30 \text{ }^{\circ}\text{C}$
- (c) $T_{\text{sat}} = 60 \text{ }^{\circ}\text{C}$

Figure 5: Boiling behavior at lower and higher heat fluxes at 30 °C.

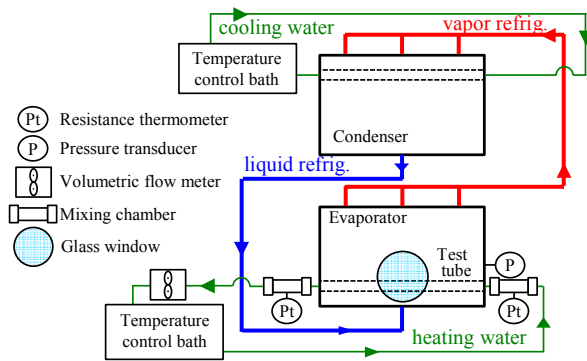
Figure 6: HTC enhancement ratio based on the plain tube. The parentheses contain the average value.

Table 1: Characteristics of the test refrigerant R1234ze(Z)

Table 2: Instrumentation and measurement uncertainties

Table 3: Dimensions of the test tubes

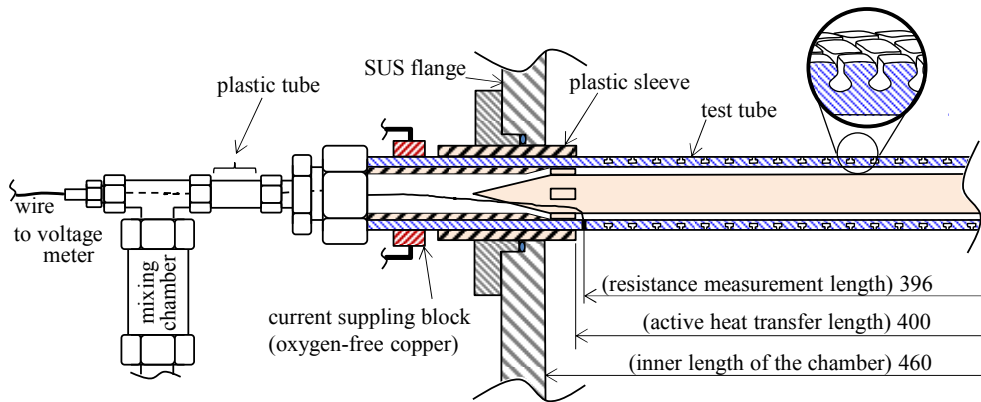
Table 4: Comparison with the predicting correlations for the plain copper and titanium tubes



(a) Water and refrigerant loop

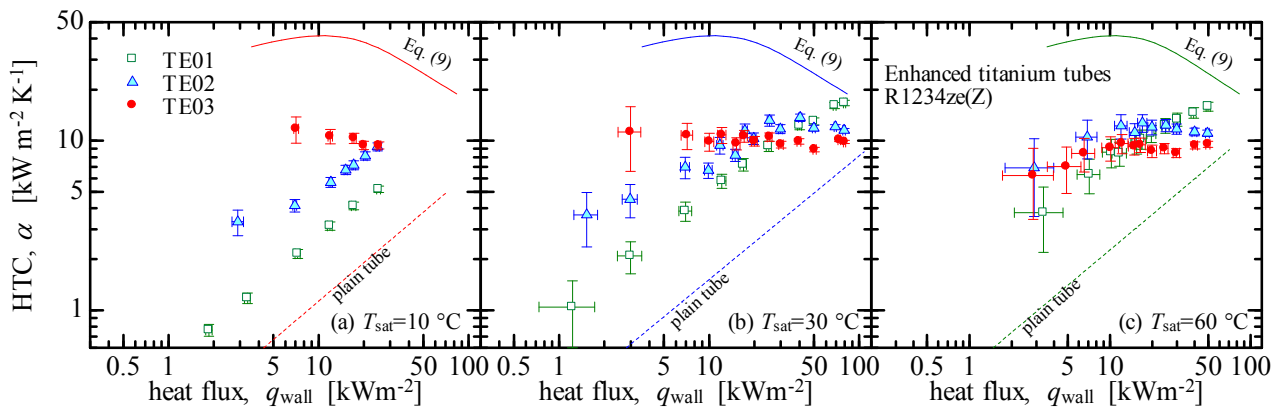
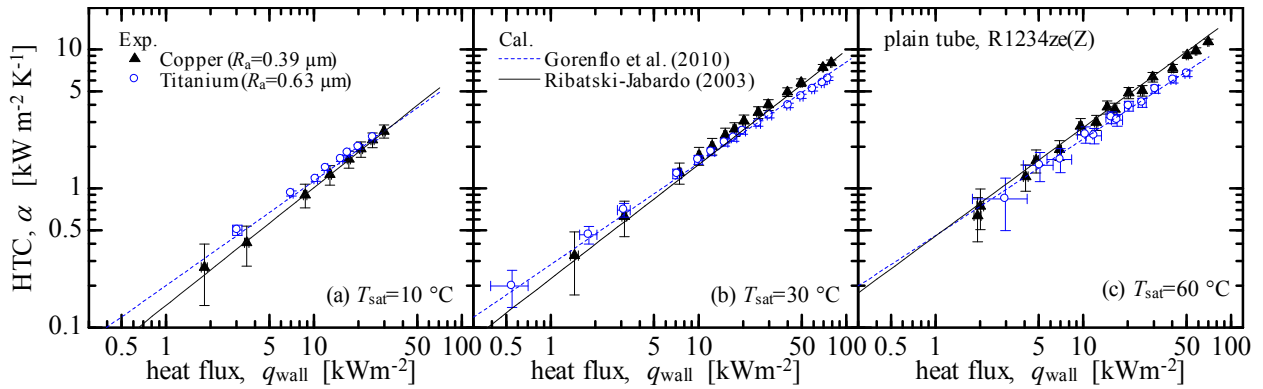
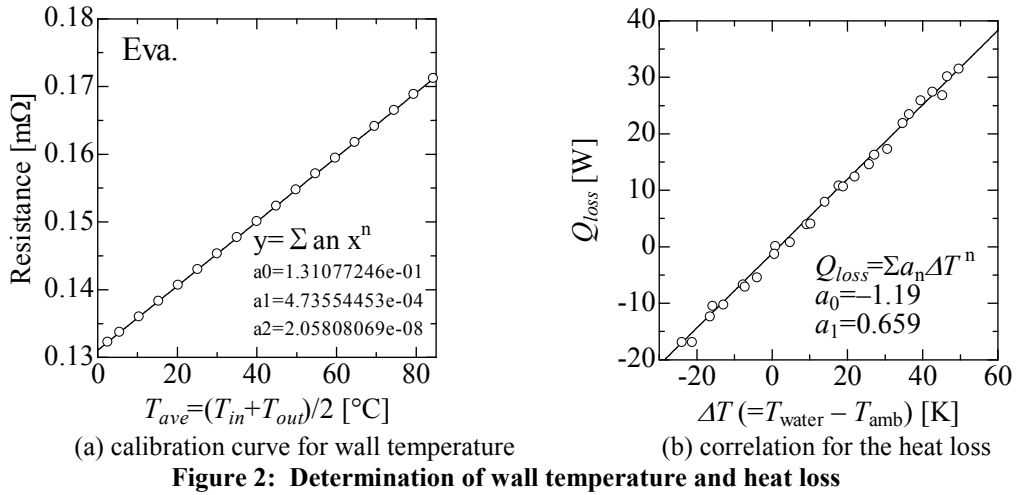


(b) The evaporator chamber without insulation



(c) Structure of the test section

Figure 1: Experimental apparatus.



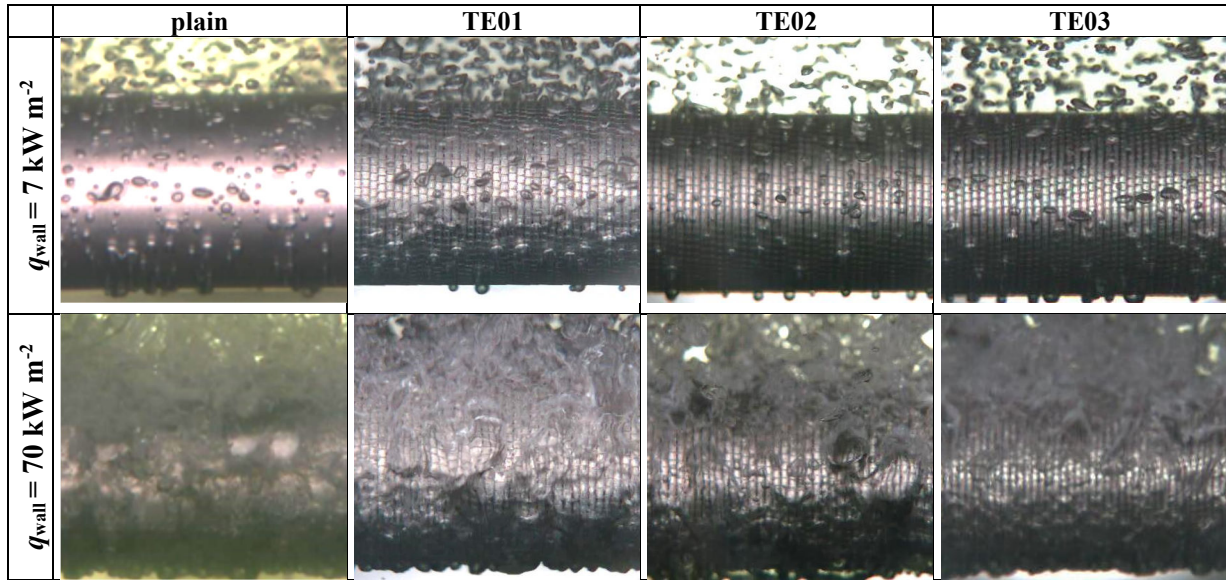


Figure 5: Boiling behavior at lower and higher heat fluxes at 30 °C.

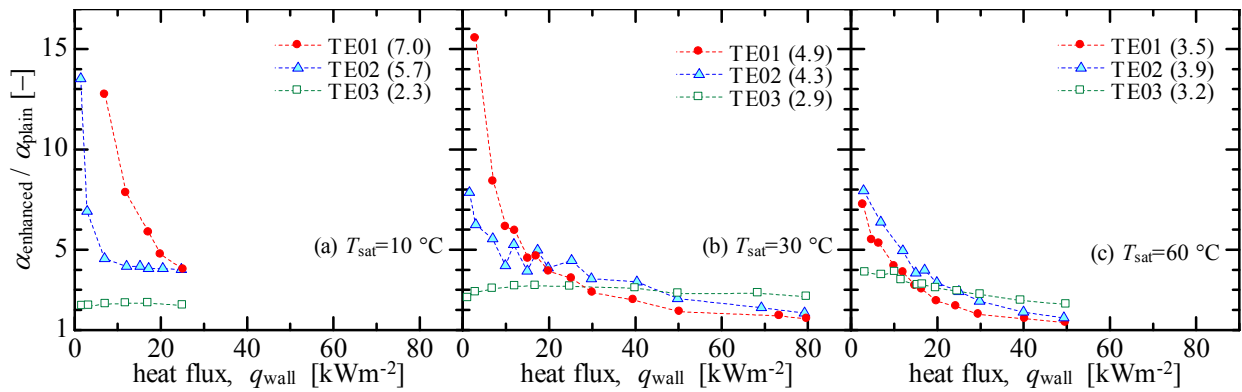


Figure 6: HTC enhancement ratio based on the plain tube. The parentheses contain the average value.

Table 1: Characteristics of the test refrigerant R1234ze(Z)

Refrigerant	R134a	R245fa	R1234ze(E)	R1234ze(Z)
chemical formula	CH ₂ FCF ₃	CF ₃ CH ₂ CHF ₂	Trans-CF ₃ CH=CHF	Cis-CF ₃ H=CHF
chemical structure				
ODP	[-]	0	0	0
GWP ₁₀₀	[-]	1300	858	<1
safety group	[-]	A1	A1	A2L (expected)
p_{crit}	[MPa]	4.059	3.651	3.635
T_{crit}	[°C]	101.1	154.0	109.4
NBP*	[°C]	-26.1	15.1	-19.0
Δh_{LV} **	[kJ kg ⁻¹]	163.0	181.14	154.8
ρ_L / ρ_V **	[kg m ⁻³]	1146.7 / 50.09	1296.7 / 14.12	1111.5 / 40.64
λ_L **	[mW m ⁻¹ K ⁻¹]	74.7	83.36	69.2
μ_L **	[μPa·s]	161.5	328.58	167.0
σ **	[mN m ⁻¹]	6.11	11.73	6.96
				10.94 (Kondou et al, 2014)

* Normal Boiling Point, ** at a saturation point of 40 °C

Table 2: Instrumentation and measurement uncertainties

Measured parameter	Instrument / Method	Uncertainty
water temperature	Sheathed Pt resistance thermometer (Yamari, ϕ 2.0mm)	±0.05 K
volumetric flow rate	gear type volumetric flow meter Oval LG45A30-G030, full scale 300 Lh ⁻¹	±0.5%RD
pressure in evaporator	absolute pressure transducer (Kyowa PHS-B-0.5 MPa)	±0.14 kPa
temperature in evaporator	K type thermocouple (Yamari, ϕ 1.0 mm)	±0.05 K
wall temperature for boiling (Cu plain)	electric resistance method	±0.084 K
wall temperature for boiling (Ti plain)	electric resistance method	±0.236 K
wall temperature for boiling (Ti 3D, TE01)	electric resistance method	±0.098 K
wall temperature for boiling (Ti 3D, TE02)	electric resistance method	±0.125 K
wall temperature for boiling (Ti 3D, TE03)	electric resistance method	±0.156 K

Table 3: Dimensions of the test tubes

	plain-Cu	plain-Ti	TE01	TE02	TE03
outer/fin tip diameter D_o , mm	19.12	19.06	18.54	18.66	18.66
inner diameter D_i , mm	16.92	15.01	15.35	15.35	15.18
wall thickness, δ , mm	1.1	2.0	1.6	1.7	1.7
fin-root diameter D_{root} , mm	-	-	16.10	17.83	15.96
surface roughness R_a , μm	0.39	0.63	-	-	-
fin height, mm		-	0.37	0.41	0.39
axial fin pitch, mm		-	0.70±0.04	0.74±0.03	0.73±0.02
circumferential fin pitch, mm		-	0.73±0.01	0.72±0.01	0.73±0.01
open mouth width		-	narrow	->	wide
thermal conductivity, λ $\text{Wm}^{-1}\text{K}^{-1}$	385	18.9	18.9	18.9	18.9

Table 4: Comparison with the predicting correlations for the plain copper and titanium tubes

	the copper tube ($N=79$)		the titanium tube ($N=36$)	
	$\bar{\varepsilon}$ [%]	S [%]	$\bar{\varepsilon}$ [%]	S [%]
Stephan-Abdelsalam (1980)	33.6	24.5	20.4	9.2
Jung et al. (2003)	8.7	17.2	-2.9	10.5
Ribatski-Jabardo (2003)	12.0	13.3	0.7	5.8
Gorenflo et al. (2010)	4.0	7.9	93.9	38.6